ChemComm

COMMUNICATION

View Article Online
View Journal | View Issue

Cite this: *Chem. Commun.*, 2015, **51**, 9636

Received 29th March 2015,
Accepted 6th May 2015

DOI: 10.1039/c5cc02573g

www.rsc.org/chemcomm

The local electric field favours more than exposed nitrogen atoms on CO_2 capture: a case study on the rht-type MOF platform†

Wen-Yang Gao,[a] Tony Pham,[a] Katherine A. Forrest,[a] Brian Space,[a] Lukasz Wojtas,[a] Yu-Sheng Chen[b] and Shengqian Ma*[a]

Two rht-type metal–organic frameworks (MOFs) based upon the tetrazolate moiety and pyrazolate moiety, respectively, have been investigated for carbon dioxide (CO_2) adsorption and selective adsorption of CO_2 over CH_4, which shows that the rht-MOF featuring the pyrazolate moiety demonstrates superior performances compared to the rht-MOF based on the tetrazolate moiety. In spite of more exposed nitrogen atoms in the tetrazolate-based rht-MOF, the counter-intuitive observations of CO_2 capture in the two rht-MOFs were interpreted by computational studies, which reveal that the local electric field favours more than the richness of exposed nitrogen atoms for the interactions with CO_2 molecules.

To capture and sequester carbon dioxide (CO_2) remains an effective route to mitigate climate change associated with anthropogenic CO_2 emission.[1] The conventional CO_2 capture technologies are dominated by the alkanolamine-based wet scrubbing systems, which feature causticity and volatility of the amines, and more prominently, high energy cost of regeneration processes.[2] It is highly needed to develop alternative approaches for CO_2 capture and sequestration. Using porous materials as adsorbents has been of great interest due to the facile regeneration process.[3] Metal–organic frameworks (MOFs)[4] have been positioned at the forefront of this area as a promising class of candidates amongst various porous materials. This is mainly triggered by the modularity and functionality of the pore size, pore walls and the inner surface of MOFs[5] by use of crystal engineering strategies.[6] In addition, the crystalline nature of MOFs can facilitate the understanding of CO_2–sorbent interactions at the molecular level, which in turn helps to design/functionalize MOFs with improved CO_2 capture performances.[7] Currently, a predominant viewpoint in this area is that accessible rich nitrogen sites as Lewis-base centers incorporated in the porous MOFs can significantly enhance CO_2 uptake capacity and selectivity on account of the dipole–quadrupole interactions. Extensive efforts thus have been devoted to increasing the density of accessible nitrogen sites within porous MOFs.[8] In this contribution, we report the investigations of CO_2 capture in two **rht**-type MOFs based upon the tetrazolate and pyrazolate moieties, which indicate some counter-intuitive results that the pyrazolate-based **rht**-MOF demonstrates superior performances compared to the tetrazolate-based **rht**-MOF featuring more exposed nitrogen atoms.

The tetrazolate-based **rht**-MOF (**rht**-MOF-1) and the pyrazolate-based **rht**-MOF (**rht**-MOF-pyr) were prepared using tetrazole- or pyrazole-derived tritopic ligands assembled with Cu(II) under the solvothermal conditions, respectively.[9] Single-crystal X-ray diffraction studies reveal that both **rht**-MOF-1 and **rht**-MOF-pyr crystallize in the same space group of $Fm\bar{3}m$. As shown in Fig. 1, $Cu_3O(N_4CR)_3$ in **rht**-MOF-1 and $Cu_3O(N_2(CH)_2CR)_3$ in **rht**-MOF-pyr serve as 3-connected nodes that link six $Cu_2(COO)_4$ paddlewheel units through six carboxylate groups of three 5-tetrazolylisophthalate or of 5-(1*H*-pyrazol-4-yl)isophthalate ligands, thus affording the classical (3,24)-connected **rht** topology network. The **rht** network is composed of three different polyhedral cages: a small rhombihexahedral cage formed by 24 functionalized isophthalate ligands linked by 12 $Cu_2(COO)_4$ paddlewheel units (Fig. 2a); a bevelled octahedral

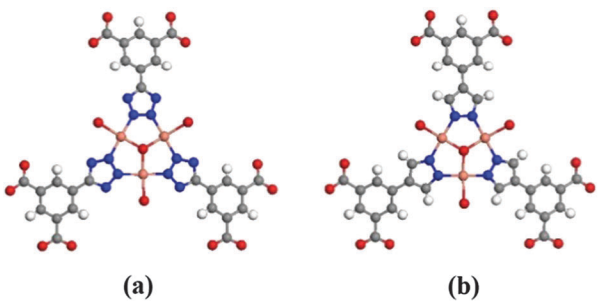

Fig. 1 Illustration of hexatopic building units of (a) **rht**-MOF-1 and (b) **rht**-MOF-pyr. Atom colors: C = gray, H = white, O = red, N = blue, and Cu = orange.

[a] *Department of Chemistry, University of South Florida, 4202 E. Flower Avenue, Tampa, Florida 33620, USA. E-mail: sqma@usf.edu; Fax: +1-813-974-3203; Tel: +1-813-974-5217*

[b] *ChemMatCARS, Center for Advanced Radiation Sources, The University of Chicago, 9700 S. Cass Avenue, Argonne, Illinois 60439, USA*

† Electronic supplementary information (ESI) available: Details of heats of adsorption for CO_2, CH_4 uptake at 273 K and 298 K of **rht**-MOF-1 and **rht**-MOF-pyr and computational studies. CCDC 922586 for **rht**-MOF-pyr. For ESI and crystallographic data in CIF or other electronic format see DOI: 10.1039/c5cc02573g

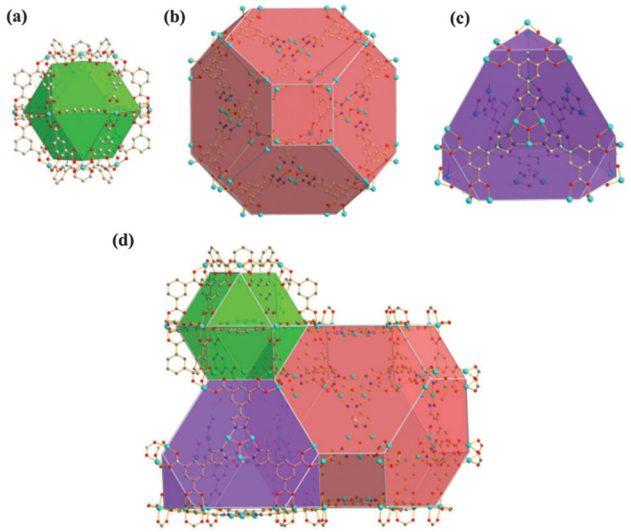

Fig. 2 Pictures of (a) rhombihexahedral cage; (b) bevelled octahedral cage; (c) bevelled tetrahedral cage and (d) close-packing of 3 types of polyhedral cages in **rht**-topology structures.

cage defined by 8 $Cu_3O(N_4CR)_3$ or $Cu_3O(N_2(CH_2)_2CR)_3$ trimers and 24 $Cu_2(COO)_4$ paddlewheel units (Fig. 2b); and a bevelled tetrahedral cage enclosed by 4 $Cu_3O(N_4CR)_3$ or $Cu_3O(N_2(CH_2)_2CR)_3$ trimers and 12 $Cu_2(COO)_4$ paddlewheel units (Fig. 2c). These multiple cages are tailored together to form 3-dimensional highly porous structures, as shown in Fig. 2d.

The phase purities of **rht**-MOF-1 and **rht**-MOF-pyr were verified by powder X-ray diffraction (PXRD) studies, which indicate that the diffraction patterns of the fresh sample are consistent with the calculated ones, as shown in Fig. S1 and S2 respectively (ESI†). Furthermore, PXRD patterns of the activated MOF samples also confirmed the consistency of their structures under the test conditions. The permanent porosity has been examined by N_2 adsorption at 77 K on both activated MOF samples (see Fig. S3 and S4, ESI†), which reveals similar BET surface areas of $\sim$2100 m^2 g^{-1} analogous to the reported values.[9]

To evaluate CO_2 uptake performances of **rht**-MOF-1 and **rht**-MOF-pyr, CO_2 adsorption isotherms were collected on the activated samples at 273 K and 298 K, as shown in Fig. 3a. **rht**-MOF-1 shows a CO_2 uptake capacity of 17.7 wt% (90.0 cm^3 g^{-1}) at 273 K and 10.7 wt% (54.5 cm^3 g^{-1}) at 298 K under the pressure of 760 Torr. In comparison, **rht**-MOF-pyr can adsorb the amount of CO_2 with an uptake capacity of 22.0 wt% (112.4 cm^3 g^{-1}) at 273 K and 13.0 wt% (66.4 cm^3 g^{-1}) at 298 K under the same pressure. This indicates a substantial and unexpected increase in CO_2 uptake capacity of 25% compared with that of **rht**-MOF-1 at 273 K. It is well documented that ligands with rich nitrogen atoms incorporated into the frameworks can polarize the adsorbed CO_2 molecules and boost the dipole–quadrupole interactions with CO_2, thus leading to the increasing CO_2 uptake capacity and selectivity. However, the observation here is counter-intuitive to this predominant viewpoint. The explanation can be presumably attributed to the different properties of tetrazole and pyrazole functional groups. The pK_a value of tetrazole is *ca.* 4.6, and comparatively that of pyrazole is *ca.* 14.0. The increasing basicity

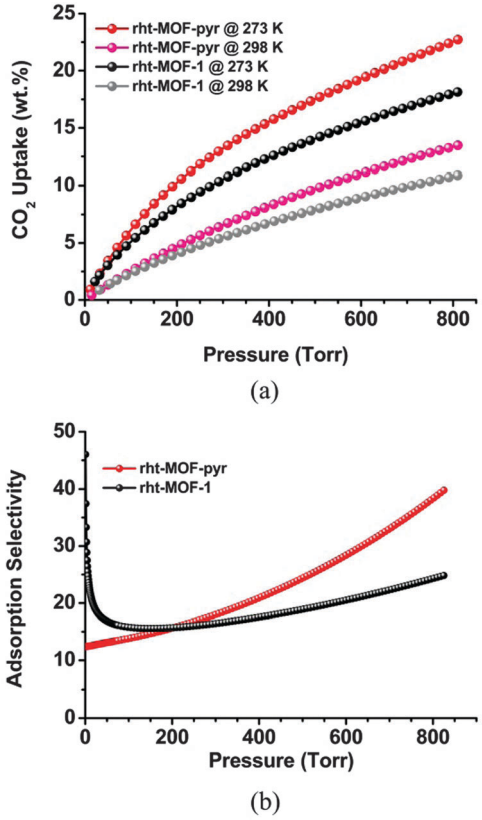

Fig. 3 (a) CO_2 adsorption isotherms of **rht**-MOF-1 and **rht**-MOF-pyr at 273 K and 298 K and (b) adsorption selectivity of CO_2 over CH_4 plots based on IAST calculations.

of azolate groups may favour the adsorption of acidic CO_2 molecules.

We also assessed the adsorption selectivity of CO_2 and CH_4 of **rht**-MOF-1 and **rht**-MOF-pyr. As shown in Fig. S6 (see ESI†), these two isostructures demonstrate comparable CH_4 uptake capacities (16.4 cm^3 g^{-1} of **rht**-MOF-1 *vs.* 17.0 cm^3 g^{-1} of **rht**-MOF-pyr at 273 K) owing to their similar surface areas. To predict the adsorption selectivity of CO_2 over CH_4, the ideal adsorption solution theory (IAST),[10] which has been validated for calculating the adsorption selectivity of gas mixtures in MOFs,[11] was employed by applying single-component adsorption isotherms. From selectivity plots of CO_2/CH_4 (50/50) shown in Fig. 3b, **rht**-MOF-pyr is calculated to exhibit an adsorption selectivity of 36 for CO_2 over CH_4 at 273 K and 1 bar, which is $\sim$56% higher than that of **rht**-MOF-1. Additionally, **rht**-MOF-1 demonstrates the peculiarly high selectivity for CO_2/CH_4 at the very low coverage. The performance can be partially interpreted by different heats of adsorption (Q_{st}) for CO_2 (see Fig. S9, ESI†). **rht**-MOF-1 exhibits $\sim$1.2 kJ mol^{-1} higher Q_{st} than that of **rht**-MOF-pyr at the very low loading of CO_2. On the other hand, the substantial discrepancy in Q_{st} for CH_4 between **rht**-MOF-pyr and **rht**-MOF-1 can also partially explain the dramatic distinction of CO_2/CH_4 selectivity at the low loading state, as shown in Fig. S12, ESI.† The Q_{st} of **rht**-MOF-1 decreases steadily over the loading range, whereas the Q_{st} of **rht**-MOF-pyr slightly increases first and then decreases across the loading range. The difference in Q_{st} for CH_4 between **rht**-MOF-pyr and

rht-MOF-1 is narrowing down, along with the increase of CH_4 loading. Other than CH_4 heats of adsorption, the favoured CO_2 interaction mode plays an essential role in **rht**-MOF-pyr at the higher loading range.

In order to gain some insights at the molecular level for these counter-intuitive observations, computational studies of CO_2 adsorption were performed on these two **rht**-MOFs. More details about the simulations performed in this work can be found in the ESI.† It was observed that the main difference in the CO_2 adsorption capacities between the two **rht**-MOFs was attributed to the difference in the CO_2 molecule interaction with the $[Cu_3O(N_{4-x}(CH)_xC–)_3]$ (x = 0 or 2) trimers in the respective MOFs. It has been well documented that electrostatic interactions have a significant impact on the adsorption properties of microporous materials and partial charges located at atomic sites are most commonly used to account for electrostatics.[12] The computational studies revealed that, as the CO_2 molecule adsorbs onto the Cu^{2+} ions of the $[Cu_3O(N_2(CH)_2C–)_3]$ trimer in **rht**-MOF-pyr, it does so such that an oxygen atom of the CO_2 molecule coordinates to a Cu^{2+} ion; simultaneously there exists an attraction between the negative charges of the oxygen atom of the CO_2 molecule and the positive charges of the nearby hydrogen atoms of the pyrazolate moieties (Fig. 4). This synchronized binding keeps the CO_2 molecule in-plane with respect to the $[Cu_3O(N_2(CH)_2C–)_3]$ trimer, thus resulting in a favorable electrostatic interaction between the CO_2 molecule and these units. In **rht**-MOF-1, the repulsion between the negative charges of the N atoms of the tetrazole groups and the negative charges of the oxygen atoms of the CO_2 molecule repels the binding of the CO_2 molecule and a Cu^{2+} ion. As a result, the CO_2 molecule is oriented at an angle and tilted out-of-plane with respect to the $[Cu_3O(N_4C–)_3]$ trimer as the CO_2 molecule is adsorbed onto the Cu^{2+} ion. This leads to a less favorable electrostatic interaction between the CO_2 molecules and the $[Cu_3O(N_4C–)_3]$ trimer in **rht**-MOF-1.

Grand canonical Monte Carlo (GCMC) simulations of CO_2 adsorption in both **rht**-MOFs confirmed that **rht**-MOF-pyr adsorbs more CO_2 than **rht**-MOF-1 for the thermodynamic conditions considered (see Fig. S14 and S15, ESI†). A radial distribution function analysis of CO_2 molecules adsorbed on different types of Cu^{2+} ions in both MOFs revealed that the Cu_3O trimer Cu^{2+} ions are occupied at higher loadings and that there is a greater population of CO_2 molecules adsorbed on such Cu^{2+} ions in **rht**-MOF-pyr relative to **rht**-MOF-1 (see Fig. S17 and S18, ESI†). Further, density functional theory (DFT) calculations confirmed that the interaction strength for CO_2 binding onto the Cu_3O trimers is greater for **rht**-MOF-pyr compared to **rht**-MOF-1 (see ESI†).

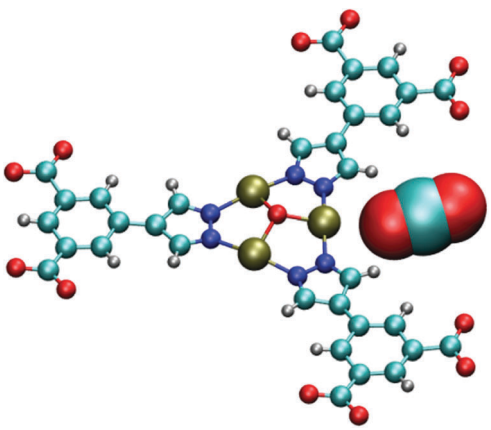

Fig. 4 Molecular illustration of the CO_2 molecule orientation about the Cu_3O trimer in **rht**-MOF-pyr as determined from molecular simulations (atom colors: C = cyan, H = white, O = red, N = blue, and Cu = gold).

Considering the host–guest (MOFs–CO_2) electrostatic interactions, the local electric field exerted by the $[Cu_3O(N_{4-x}(CH)_xC–)_3]$ (x = 0 or 2) trimer units thus plays a more dominant role than the exposed nitrogen atoms for the interactions with CO_2 molecules on the **rht**-MOF platform. More importantly, the synergistic electrostatic effects from the neighboring atoms/moieties should be taken into account leading to more precise and accurate results. Hence, we can conclude that the essential factors influencing CO_2 adsorption behind the effect of exposed nitrogen sites lie in the local electric fields, instead of the number of accessible nitrogen atoms. Furthermore, it can be observed that the Q_{st} for CO_2 in **rht**-MOF-pyr surpasses that of **rht**-MOF-1 with the increase of the CO_2 loading amount, which therefore must be attributed to the difference in the CO_2 binding energies with the $[Cu_3O(N_{4-x}(CH)_xC–)_3]$ (x = 0 or 2) trimers within the two **rht**-MOFs. Computational studies demonstrate that the absorbed CO_2 molecules preferentially interact with the Cu atoms of paddle wheel units, instead of trimer units at the low loading range. Furthermore, **rht**-MOF-1 has a low electron density than **rht**-MOF-pyr on the Cu atoms of paddle wheel units, which increases the CO_2 bonding strength to the Cu atoms of **rht**-MOF-1.[9b] This is also in line with the Q_{st} of CO_2 at the low loading range that **rht**-MOF-1 shows higher heats of adsorption than **rht**-MOF-pyr. However, when the copper sites of paddle wheel units saturated with CO_2 molecules, Q_{st} of **rht**-MOF-pyr turns to be higher than that of **rht**-MOF-1, owing to the CO_2 molecule subsequently interacting with the trimer units. Therefore, the modeling results presented in this work are consistent with the experimentally observed CO_2 Q_{st} values for the two MOFs.

In summary, we investigated the performances in CO_2 adsorption and selective adsorption of CO_2 over CH_4 for the prototypal **rht**-MOF platform functionalized by tetrazolate and pyrazolate moieties. Our studies revealed that **rht**-MOF-pyr lacking exposed nitrogen atoms demonstrated better CO_2 capture performances than **rht**-MOF-1 rich in exposed nitrogen atoms. The counter-intuitive experimental observations have been well elucidated by computational studies, which reveal that the local electric field favours more than the richness of exposed nitrogen atoms for the interactions with CO_2 molecules. Our work therefore provides a new perspective for future design of new MOFs and other types of porous materials with improved performances for applications in CO_2 capture and gas storage/separation.

The authors acknowledge National Science Foundation (DMR-1352065) and University of South Florida for financial support of this work. B. S. acknowledges the National Science Foundation (Award No. CHE-1152362) and the computational resources that were made available by an XSEDE Grant (No. TG-DMR090028). The single-crystal X-ray diffraction of **rht**-MOF-pyr was carried out at ChemMatCARS Sector 15-ID-B, supported by the National Science Foundation under grant number NSF/CHE-1346572. This research

used resources of the Advanced Photon Source, a U.S. Department of Energy (DOE) Office of Science User Facility operated for the DOE Office of Science by Argonne National Laboratory under Contract No. DE-AC02-06CH11357.

Notes and references

1 (*a*) S. Chu, *Science*, 2009, **325**, 1599; (*b*) J.-R. Li, Y. Ma, M. C. McCarthy, J. Sculley, J. Yu, H.-K. Jeong, P. B. Balbuena and H.-C. Zhou, *Coord. Chem. Rev.*, 2011, **255**, 1791.

2 (*a*) J. Johnson, *Chem. Eng. News*, 2004, **82**, 36; (*b*) J. Liu, P. K. Thallapally, B. P. McGrail, D. R. Brown and J. Liu, *Chem. Soc. Rev.*, 2012, **41**, 2308.

3 (*a*) A.-H. Lu and G.-P. Hao, *Annu. Rep. Prog. Chem., Sect. A: Inorg. Chem.*, 2013, **109**, 484; (*b*) Y. Zhang, B. Li, K. Williams, W.-Y. Gao and S. Ma, *Chem. Commun.*, 2013, **49**, 10269; (*c*) M. R. Hudson, W. L. Queen, J. A. Mason, D. W. Fickel, R. F. Lobo and C. M. Brown, *J. Am. Chem. Soc.*, 2012, **134**, 1970; (*d*) S. Xiang, Y. He, Z. Zhang, H. Wu, W. Zhou, R. Krishna and B. Chen, *Nat. Commun.*, 2012, **3**, 954; (*e*) P. Nugent, Y. Belmabkhout, S. D. Burd, A. J. Cairns, R. Luebke, K. Forrest, T. Pham, S. Ma, B. Space, L. Wojtas, M. Eddaoudi and M. J. Zaworotko, *Nature*, 2013, **495**, 80; (*f*) A. I. Cooper, *Adv. Mater.*, 2009, **21**, 1291; (*g*) W. Lu, J. P. Sculley, D. Yuan, R. Krishna, Z. Wei and H.-C. Zhou, *Angew. Chem., Int. Ed.*, 2012, **51**, 7480; (*h*) D.-S. Zhang, Z. Chang, Y.-F. Li, Z.-Y. Jiang, Z.-H. Xuan, Y.-H. Zhang, J.-R. Li, Q. Chen, T.-L. Hu and X.-H. Bu, *Sci. Rep.*, 2013, **3**, 3312; (*i*) S.-M. Zhang, Z. Chang, T.-L. Hu and X.-H. Bu, *Inorg. Chem.*, 2010, **49**, 11581.

4 (*a*) H.-C. Zhou, J. R. Long and O. M. Yaghi, *Chem. Rev.*, 2012, **112**, 673; (*b*) K. Sumida, D. L. Rogow, J. A. Mason, T. M. McDonald, E. D. Bloch, Z. R. Herm, T.-H. Bae and J. R. Long, *Chem. Rev.*, 2012, **112**, 724; (*c*) H.-C. Zhou and S. Kitagawa, *Chem. Soc. Rev.*, 2014, **43**, 5415.

5 (*a*) J. J. Perry, J. A. Perman and M. J. Zaworotko, *Chem. Soc. Rev.*, 2009, **38**, 1400; (*b*) H. Furukawa, K. E. Cordova, M. O'Keeffe and O. M. Yaghi, *Science*, 2013, **341**, 1230444; (*c*) W. Lu, Z. Wei, Z.-Y. Gu, T.-F. Liu, J. Park, J. Park, J. Tian, M. Zhang, Q. Zhang, T. Gentle III, M. Bosch and H.-C. Zhou, *Chem. Soc. Rev.*, 2014, **43**, 5561; (*d*) W.-Y. Gao, M. Chrzanowski and S. Ma, *Chem. Soc. Rev.*, 2014, **43**, 5841; (*e*) W.-Y. Gao and S. Ma, *Comments Inorg. Chem.*, 2014, **34**, 125.

6 (*a*) G. R. Desiraju, *Crystal Engineering: The Design of Organic Solids*, Elsevier, Amsterdam, 1989; (*b*) O. M. Yaghi, M. O'Keeffe, N. W. Ockwig, H. K. Chae, M. Eddaoudi and J. Kim, *Nature*, 2003, **423**, 705.

7 (*a*) R. Vaidhyanathan, S. S. Iremonger, G. K. H. Shimizu, P. G. Boyd, S. Alavi and T. K. Woo, *Science*, 2010, **330**, 650; (*b*) P.-Q. Liao, D.-D. Zhou, A.-X. Zhu, L. Jiang, R.-B. Lin, J.-P. Zhang and X.-C. Ming, *J. Am. Chem. Soc.*, 2012, **134**, 17380; (*c*) N. C. Burtch, H. Jasuja, D. Dubbeldam and K. S. Walton, *J. Am. Chem. Soc.*, 2013, **135**, 7172; (*d*) O. Shekhah, Y. Belmabkhout, Z. Chen, V. Guillerm, A. Cairns, K. Adil and M. Eddaoudi, *Nat. Commun.*, 2014, **5**, 4228; (*e*) J.-P. Zhang, P.-Q. Liao, H.-L. Zhou, R.-B. Lin and X.-M. Chen, *Chem. Soc. Rev.*, 2014, **43**, 5789.

8 (*a*) J. An, S. J. Geib and N. L. Rosi, *J. Am. Chem. Soc.*, 2010, **132**, 38; (*b*) J. An and N. L. Rosi, *J. Am. Chem. Soc.*, 2010, **132**, 5578; (*c*) W.-Y. Gao, W. Yan, R. Cai, K. Williams, A. Salas, L. Wojtas, X. Shi and S. Ma, *Chem. Commun.*, 2012, **48**, 8898; (*d*) Q. Lin, T. Wu, S.-T. Zheng, X. Bu and P. Feng, *J. Am. Chem. Soc.*, 2012, **134**, 784; (*e*) R. Luebke, Ł. J. Weseliński, Y. Belmabkhout, Z. Chen, L. Wojtas and M. Eddaoudi, *Cryst. Growth Des.*, 2014, **14**, 414.

9 (*a*) F. Nouar, J. F. Eubank, T. Bousquet, L. Wojtas, M. J. Zaworotko and M. Eddaoudi, *J. Am. Chem. Soc.*, 2008, **130**, 1833; (*b*) W.-Y. Gao, R. Cai, T. Pham, K. A. Forrest, A. Hogan, P. Nugent, K. Williams, L. Wojtas, R. Luebke, L. J. Weselinski, M. Eddaoudi, M. J. Zaworotko, B. Space, Y.-S. Chen, X. Shi and S. Ma, *Chem. Mater.*, 2015, **27**, 2144.

10 A. L. Myers and J. M. Prausnitz, *AIChE J.*, 1965, **11**, 121.

11 (*a*) Y.-S. Bae, K. L. Mulfort, H. Frost, P. Ryan, S. Punnathanam, L. J. Broadbelt, J. T. Hupp and R. Q. Snurr, *Langmuir*, 2008, **24**, 8592; (*b*) J. A. Mason, K. Sumida, Z. R. Herm, R. Krishna and J. R. Long, *Energy Environ. Sci.*, 2011, **4**, 3030.

12 (*a*) R. Krishna, *Chem. Soc. Rev.*, 2012, **41**, 3099; (*b*) M. Fisher and R. G. Bell, *J. Phys. Chem. C*, 2013, **117**, 24446.